Proceedings of 20th International Congress on Acoustics, ICA 2010

23-27 August 2010, Sydney, Australia

Computation of drag and flow noise along wavy wall in turbulent flow

Huaixin Zhang (1), Kunyu Meng (1) and Yonglin Shi (1)

(1) School of Naval Architecture, Ocean and Civil Engineering, Shanghai Jiaotong University

Shanghai , 200030, China

PACS: 43.28.RA

ABSTRACT

In this paper, a numerical simulation of flow-induced noise by the low Mach numbers, the turbulent flow with a sinusoidal wavy wall is presented based on the unsteady incompressible Navier-Stokes equations and Lighthill's acoustic analogy. Large Eddy Simulation (LES) was used to investigate space-time flow field and the Smagorinsky sub-grid scale (SGS) model was introduced for turbulence model. Using Lighthill's acoustics analogy, the flow field simulated by LES was taken as near-field sound sources and radiated sound from turbulent flow was computed by Curle's integral formulation under the low-mach-number approximation. The relationship between flow noise and drag on the wavy wall is studied. Which kind of spanwise wavy wall or streamwise wavy wall with various wall wave amplitude could get the effect on reducing drag and flow noise are discussed.

1. INTRODUCTION

The control of the near-wall coherent structures is of great importance for various engineering applications since many researches show that some wall surface with micro-grooves, so called riblets, aligned in the flow direction presents the advantage of reducing the drag. Although the riblets are recognized as a successful device, at least, or the drag reduction purpose, the mechanism responsible is not fully clear and neither wall geometry optimization nor the effect to reduce flow noise has been made up to the present. In order to improve dynamical performance and reduce the acoustic noise, a very attractive issue is whether it is possible to obtain a wall geometry that reduces a skin drag coefficient and radiated sound from turbulent flow.

The wavy wall's effect of drag and noise reduction has been widely studied by many researchers over the past few decades. Initial studies into the drag reduction with the use of riblets were conducted by Walsh[1] and his colleagues at NASA Langley Research Center, whose researches were devoted to optimize the riblet size and shape for a maximum drag reduction. The result shows that the V-type grooves with a height to length ratio in 25~30 has a better frictional drag reduction in the range of 4-8%. This issue attracts widely interests and researchers are studying the effects of riblets on near-wall drag by experiments or numerical simulations. Park, Wallace[2] said that the flow within the riblet valleys is strongly dominated by viscosity. Choi[3] concluded that such drag reduction occurs only in turbulent region, while a drag increase is in variably obtained in laminar conditions. On the other hand, Bechert[4] whose study was focusing on experiments has investigated more thoroughly different configurations of riblets including rectangular, scalloped and shark-skin-shape riblets. Although numerical techniques had lagged the experiments due to the lack of the computational resources, it can be used for more complex configurations when more parameters are to be discussed such as the riblet amplitude and lengths.

Flows along both spanwise and streamwise wavy walls display peculiar characteristics that are not observed in the flows over a flat plate surface. In the case of wavy wall flows, the periodic changes of pressure gradient and of streamline curvature generate turbulence structure different from the counterpart of flat plate flows, but the effects to reduce drag and flow noise are not same on spanwise and streamwise wavy walls. Many studies show that the spanwase wavy wall vertical to the stream flow direction is effective. On the basis of the coherent structure theory, It was proposed that the drag reducing grooved surface can not only control the spaces between two low-speed streaks to further reduce turbulent burst frequency, but also make a part or the whole quiet fluid in grooves avoid encountering the high-speed fluid from the upper layer downwash and a higher shear stress induced by it. Thus, turbulent drag reduction can be achieved. But the research about streamwise wavy wall is very few. In this paper, which kind of spanwise wavy wall or streamwise wavy wall with various wall wave amplitude could get the effect on reducing the skin drag and the flow noise are discussed.

This paper is composed of four parts. Section 2 is devoted to a brief discussion of the theory of the Large Eddy Simulation (LES) and the Lighthill's acoustics analogy which would be used in this study. The computational model of the wavy wall in the turbulent flow is to be described in Section 3.

Results of the drag and flow-induced noise on both spanwise and streamwise wavy wall are provided in Section 4. Also, there will be some analysis focusing on why the wavy wall can reduce the drag and the flow noise.

2. Basic Theory

2.1 Large Eddy Simulation method

The LES method partitions the turbulent flow into two parts by the grid filtering operation. The large-scale eddies, generated by the instability of the mean flow, are responsible for most of the transport of momentum, mass, and other scalars. The small-scale eddies (subgrid-scale), generated by the energy-cascade process from larger eddies, are contribute little to heat and momentum transport, but have flux and feed-back effects on the large-scale flow. According to these assumptions, the larger structures can be simulated directly by the filtered N-S equations and the smaller one should be described approximately by using the Smagorinsky sub-grid scale model.

The filtering operation is defined by:

$$\overline{f}(\boldsymbol{x},t)=\int_D \overline{G}(\boldsymbol{x},\boldsymbol{x}',\Delta) f(\boldsymbol{x}',t)d\boldsymbol{x}' \qquad (1)$$

where D is the computational domain, $\overline{G}$ is the filter function and Δ is the filter width, usually we use the box type. The spatially filtered continuity equation and the incompressible N-S equation can be written in Cartesian tensor notation as follows:

$$\frac{\partial \overline{u}_i}{\partial x_i}=0 \qquad (2)$$

$$\frac{\partial \overline{u}_i}{\partial t}+\frac{\partial}{\partial x_j}(\overline{u}_i\overline{u}_j)=-\frac{1}{\rho}\frac{\partial \overline{p}}{\partial x_i}+\nu\frac{\partial^2 \overline{u}_i}{\partial x_j^2}-\frac{\partial}{\partial x_j}\tau_{ij}^S \qquad (3)$$

where $\overline{u}_i$ is the large scale relative velocity (or mean velocity) component, $\tau_{ij}^S=\overline{u}_i\overline{u}_j-\overline{u_iu_j}$ is the subgrid scale (SGS) stress tensor $(i,j=1,2,3)$.

The subgrid scale stress τ_{ij}^S is the reflection of the interaction between the large eddies and the small, such as the energy and momentum transportation and the feed-back effect on large eddies. It is always modeled by a Smagorinsky type eddy-viscosity model as follows:

$$\tau_{ij}^S-\frac{1}{3}\delta_{ij}\tau_{kk}=\nu_T\left(\frac{\partial \overline{u_i}}{\partial x_j}+\frac{\partial \overline{u_j}}{\partial x_i}\right)=2\nu_T\overline{S_{ij}} \qquad (4)$$

where ν_T is the subgrid eddy viscosity coefficient, δ_{ij} is the Kronecker symbol and $\overline{S_{ij}}$ is the resolved-scale strain rate tensor, in which

$$\overline{S_{ij}}=\frac{1}{2}\left(\frac{\partial \overline{u_i}}{\partial x_j}+\frac{\partial \overline{u_j}}{\partial x_i}\right) \qquad (5)$$

The eddy viscosity ν_T is defined as

$$\nu_T=\left(C_s\overline{\Delta}\right)^2\left|\overline{S}\right| \qquad (6)$$

where $\left|\overline{S}\right|=\left(2\overline{S_{ij}S_{ij}}\right)^{1/2}$ is the magnitude of $\overline{S_{ij}}$. The filter width $\overline{\Delta}=(\overline{\Delta}_x,\overline{\Delta}_y,\overline{\Delta}_z)^{1/3}$, where $\overline{\Delta}_x$, $\overline{\Delta}_y$ and $\overline{\Delta}_z$ are the grid spacing in the $\boldsymbol{x}$, $\boldsymbol{y}$ and $\boldsymbol{z}$ directions, respectively. The model coefficient C_s is the Smagorinsky constant, in this study, it is chosen to be 0.1. Thus, since we have modeled the SGS stress τ_{ij}^S, the Large Eddy Simulation can be enforced by equation (2) and (3).

2.2 Lighthill's acoustic analogy

Lighthill's acoustic analogy[5] forms the starting point for the derivation of the flow-induced noise prediction. The acoustic wave equation relates the sound propagation and the noise generation. We can get the sound propagation process and the change of the sound pressure at observation points in far-field approximately from it. The Lighthill's equation is derived from the continuity equation and the N-S equations in the Cartesian tensor form:

$$\left[\frac{\partial^2}{\partial t^2}-c_0^2\frac{\partial^2}{\partial x_j\partial x_j}\right]\rho'=\frac{\partial^2 T_{ij}}{\partial x_i\partial x_j} \qquad (7)$$

where $\rho'=\rho-\rho_0$ is the density fluctuation, ρ_0 is the free-stream density of fluid, c_0 is the sound speed in water under undisturbed conditions. T_{ij} is the Lighthill's stress tensor which is defined as

$$\begin{aligned} T_{ij}&=\rho u_iu_j-p_{ij}-\delta_{ij}c_0^2(\rho-\rho_0)\\ p_{ij}&=-p\delta_{ij}+\tau_{ij}, \end{aligned} \qquad (8)$$

In above equation, p_{ij} is the stress tensor, p is the static pressure, δ_{ij} is the Kronecker symbol and $\tau_{ij}=\mu(\frac{\partial u_i}{\partial x_j}+\frac{\partial u_j}{\partial x_i}-\frac{2}{3}\delta_{ij}\frac{\partial u_k}{\partial x_k})$ is the viscous part of Stokes stress tensor.

Because the hydrodynamic and acoustic terms in equation (7) are coupled each other, which makes we couldn't get an accurate answer from (7), we should make some assumptions that the coupling is neglected in low Mach flow, and then the source terms in the right side of equation (7) can be seen as known quantities from the flow field.

If solid surface exists in the sound source region, Curle[6] derived a simple solution for noise produced by the rigid surface moving through a quiescent medium

$$\begin{aligned} \rho(\boldsymbol{x},t)-\rho_0=-\frac{1}{4\pi xc_0^2}\Big(&\frac{\partial}{\partial x_i}\int_S\frac{n_ip_{ij}(\boldsymbol{y},t-|\boldsymbol{r}|/c_0)}{|\boldsymbol{r}|}d^2\boldsymbol{y}\\ &-\frac{\partial^2}{\partial x_ix_j}\int_V\frac{T_{ij}(\boldsymbol{y},t-|\boldsymbol{r}|/c_0)}{|\boldsymbol{r}|}d^3\boldsymbol{y}\Big) \end{aligned} \qquad (9)$$

where $\boldsymbol{x}$ and $\boldsymbol{y}$ represent the position vectors of the observer and the sources, respectively, $|\boldsymbol{r}|=|\boldsymbol{x}-\boldsymbol{y}|$, $|\boldsymbol{r}|/c_0$ is called the delay time and represents the time interval of sound wave

traveling from the sound sources to the observer, n_j represents the vector normal to the rigid surface S over which the surface integration is taken place. The far-field is defined by $|\boldsymbol{r}| >> l_e / M$, where l_e is the typical eddy size, $M = U/c_0$ is the freestream Mach number.

To simplify equation (9), all variables, such as ρ, $\boldsymbol{r}$ and t can be non-dimensionalized by a characteristic length L, and the inflow velocity U. Furthermore, if the solid surface and the unsteady flow region are small compared with the typical acoustic wavelength l_e / M, a compact sound source can be assumed, so that the far-field density can be approximated. Finally, we obtain

$$\rho(\boldsymbol{x},t)-1=\frac{M^3}{4\pi}\frac{x_i}{x^2}\frac{\partial}{\partial t}\int_S n_j p_{ij}(\boldsymbol{y},t)d^2\boldsymbol{y} + \frac{M^4}{4\pi}\frac{x_i x_j}{x^3}\frac{\partial^2}{\partial t^2}\int_V T_{ij}(\boldsymbol{y},t)d^3\boldsymbol{y} \quad (10)$$

In equation (10), the first term represents a dipole sound source and the second term shows a quadrupole sound source, which respectively represent the compact surface and volume sound radiation. The pressure fluctuations and viscous shear tensors on the wall boundary generate sound radiation of dipole type, the Lighthill's stress tensor behave as quadrupole. In low Mach number condition, the first term dominates, and sometimes the second term could be neglected.

3. Computational Model

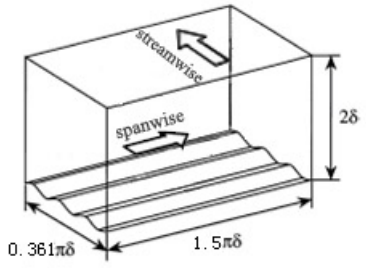

Figure 1. Computational domain

Fig. 1 shows the computational domain. An infinite board is placed in the water. In this study, the length of $\boldsymbol{x}$, $\boldsymbol{y}$ and $\boldsymbol{z}$ direction are $0.361\pi\delta \times 2\delta \times 1.5\pi\delta$, respectively, where $\delta = 0.05$ is the boundary layer thickness of the plate. The inflow is at a rate of 5m/s in the direction of $-\boldsymbol{z}$ and the two sides along $\boldsymbol{z}$ direction of the plate are assumed to be symmetry. Computation has been made for three cases: spanwise, streamwise wavy walls and flat plate which for comparison. We describe the wavy wall as the sinusoidal undulation having a amplitude a and wavelength λ. For spanwise wavy wall case, the amplitude to wavelength ratio of wall undulation a/λ is 1/20, 1/12, 1/8, 1/6 and 1/4. And for streamwise wavy wall case, amplitude to wavelength ratio of wall undulation a/λ is 1/200, 9/180, 1/80 and 3/200. The specific characteristics of these models are listed in Tab. 1 and 2. For example, the wave curve equation of model can be written as:

$$y = a\sin\frac{2\pi}{\lambda}(x-a)+a \quad (11)$$

In the acoustic computation part, the observation point at far-field was chosen to be (0m, 0.5m, 0m). To get the higher frequency parts of the flow-induced noise, we use 0.0001 as the time step. Acoustic data collection will be taken place after a period of time when the flow-field has become statistically steady.

Table 1. Specific characteristics of spanwise wavy wall

SP	01	02	03	04	05
a(m)	2.8375e-4	2.8375e-4	2.8375e-4	2.8375e-4	2.8375e-4
λ(m)	1.1350e-3	1.7025e-3	2.2700e-3	3.4050e-3	5.6750e-3
a/λ	1/4	1/6	1/8	1/12	1/20

Table 2. Specific characteristics of streamwise wavy wall

ST	001	002	003	004
a(m)	5.675e-06	1.277e-05	1.419e-05	1.703e-05
λ(m)	1.135e-03	1.135e-03	1.135e-03	1.135e-03
a/λ	1/200	9/800	1/80	3/200

4. Numerical Results

The simulation results of this study can be divided into two parts: case of spanwise and streamwise wavy wall, which will be shown in 4.1 and 4.2, respectively. Also, there are two steps in each case, the result of drag and the flow-induced noise.

4.1 Case of Spanwise wavy wall

4.1.1 Drag results of spanwise wavy wall

In this case, in order to find models which have the best effect on drag reduction, we have tried many models with different a/λ values and finally found five wavy walls as listed in Tab. 1. We also investigate a flat plate's (called SP-00) drag and noise performance as comparisons. And we obtain the drag of these 6 models as is listed in Tab. 3:

Table 3. Drag results of spanwise wavy wall

SP	a/λ	Pressure drag(N)	Frictional drag(N)	Total drag(N)	Total coefficient
00	--	0.0000E+00	4.6655E-01	4.6655E-01	2.7960E-03
01	1/4	8.0800E-10	3.5987E-02	3.5990E-02	2.1571E-03
02	1/6	8.6800E-11	5.7907E-02	5.7910E-02	2.3139E-03
03	1/8	6.4000E-10	8.0509E-02	8.0510E-02	2.4128E-03
04	1/12	1.9900E-09	1.2842E-01	1.2842E-01	2.5659E-03
05	1/20	4.6800E-09	2.3162E-01	2.3162E-01	2.7761E-03

Then, we have the relationship between a/λ and the total coefficient as shown in Fig. 2:

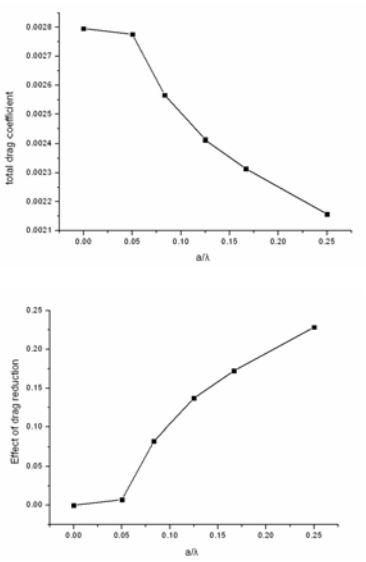

Figure 2. Total drag coefficient and effect of drag reduction results of spanwise wavy wall

The effect of drag reduction factor ε_D can be defined as:

$$\varepsilon_D = \frac{D_{flat} - D_{wavy}}{D_{flat}} \qquad (12)$$

where D_{flat} and D_{wavy} are the total drag of the flat plate and wavy wall, respectively. The curve of $a/\lambda - \varepsilon_D$ are drawn in Fig. 2.

From Fig. 2, we can explicity see that the model SP-05 has the worst effect of drag reducing capability, while SP-01 is the best. And as the wave amplitude to length ratio a/λ increased, the effect factor ε_D become obviously more higher. According to our study, the length and amplitude of the wavy should be restricted in a suitable range, otherwise, there will be a different result.

Since we have already found a group of wavy wall models that can reduce the drag, and there are some regular things we can find from Fig. 2. Now our question is that why the wavy surfaces have these effects. For this phenomenon, scientists have proposed many kinds of hypotheses while there isn't a convinced description. Bacher's "quadratic-vortex" theory, which has wide-range influence, believes that the interaction between the turbulent flow and top of the micro-grooves or riblets forms quadratic-vortexes. The quadratic-vortex, as shown in Fig. 3, which has reverse direction to the spanwise-vortex, not only weaken the intensity of the spanwise-vortex, but also hold the flow quiet and make it have lower velocity in the grooves.

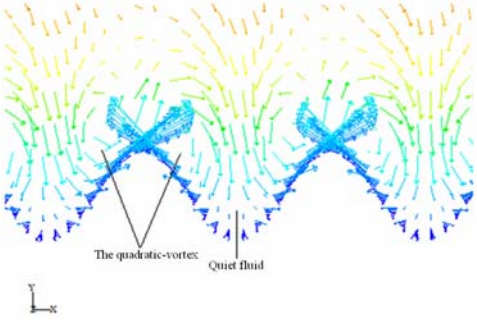

Figure 3. The quadratic-vortex

Combined with this theory, we can explain our wavy wall results from two aspects: the wall shear stress and velocity component. The average shear stress of the flat plate, as is shown in Fig. 4, is the largest one (34.9 Pa), while model SP-05 is lower than it, followed by SP-01. This resulted in a drag distinction and directly explained why SP-01 has the best effect. From Fig. 4 we can also see that the appearing regions of these three models' surface high stress are different, where the flat plat has an average distribution of shear stress, and the other two's are mainly concentrated in the top of the grooves, which indicates that there have bigger frictional drag.

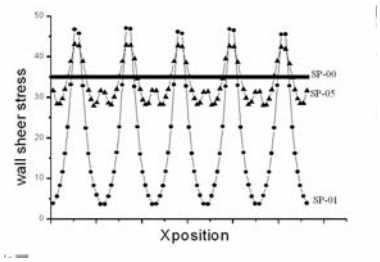

Figure 4 Wall shear stress of 3 models in case of spanwise

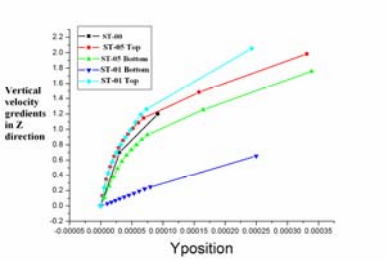

Figure 5 Vertical Velocity gradients of 3 models in case of spanwise

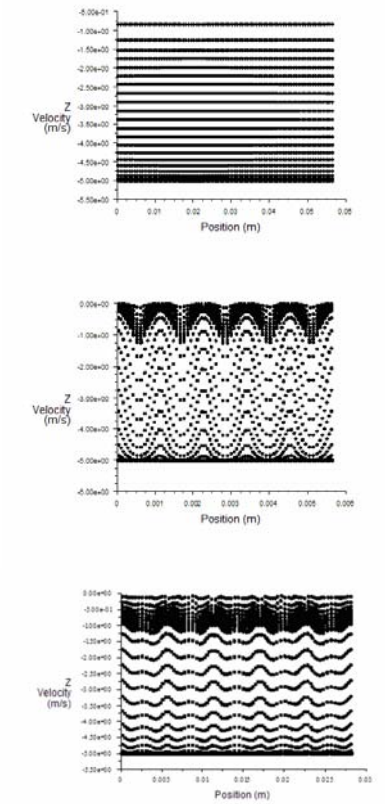

Figure 6.Velocity distributions along spanwise of SP-00, 01 and 05

Fig. 5 shows the vertical velocity distribution in Y-Z plane and Fig. 6 shows the velocity distribution of these three models. The flat plate's velocity distribution along spanwise is smooth and average, while SP-01 and 05 obviously express as wave-shape, which bottom of the groove has a thick viscous layer and the velocity gradients there are very small. This situation could be seen more clearly in Fig. 5. Compared with 00 and 01, the velocity gradients in the top of model SP-01 are a bit bigger than it in the flat plate, but in the middle and bottom of the groove the gradients are much lower. It means that in this area of the wavy wall's groove there are very large quantity of the lower-velocity fluid, which extremely decreased the velocity fluctuation and the frequency of the moment exchanging. These facts explain why the shear stress in the groove is small.

Considering about model SP-01 and 05, we can see that although SP-05's total drag is larger than 01', the maximum of these two models' shear stresses are different, with the value of 43.1Pa and 47.3Pa, respectively. The reason is that the location of the quadratic-vortex in model SP-05 is the lowest and the high-intensity fluid's momentum transportation is the strongest, which induces a larger area of high-stress zone. Further more, because the slope of SP-05's wall curve is small, which means the fluid near the groove bottom is blocked and the volume of quiet flow is less than other wavy walls, these things made it have bigger drag than SP-01.

From all these analysis, we can conclude that the existence of the quadratic-vortex can hold the flow quiet and make it have a low speed. It is the main reason of drag reduction. Further more, with the top of groove's slope decreasing, the effects with surrounding fluid are becoming intensity, and the strength of the quadratic-vortex which is generated in the middle and upper of groove also grows higher, so that it brings two aspects of influences: first, which is also the dominant one, the local shear stresses are let down because of the reducing of velocity gradients. Second, the middle and upper flow's velocity gradients are becoming larger, which made the shear stress goes up. Since the first aspect's influence is larger, the total shear stresses are decreased and then lead the drag reduced.

4.1.2 Acoustic results of spanwise wavy wall

The acoustic computation is executed based on the results of an unsteady computation by using the information of the flow-field. During this process, we used Lighthill's acoustic analogy to simulate the numerical model. Sound pressure (in db) and power density results are shown in Fig. 7:

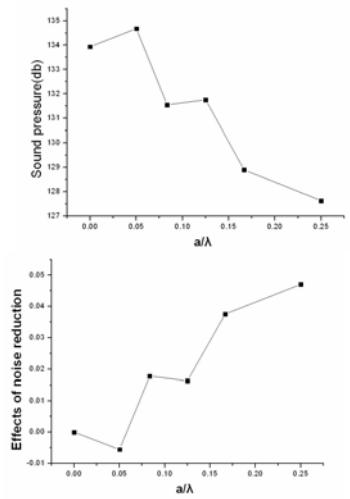

Figure 7 Sound pressure and the effect of noise reduction results of spanwise wavy wall

The effect of noise reduction coefficient η_P is defined as

$$\eta_P = \frac{P_{flat} - P_{wavy}}{P_{flat}}$$

where P_{flat}, P_{wavy} are the sound pressure of the flat plate and wavy plate, respectively. From these two pictures we can find that all the models' sound pressure exists in a reasonable range and each of them doesn't have large variation. Although this effect is small, we also can see the trend that as the value of a/λ increased, η_P will be non-strictly become higher. The following pictures (Fig. 8~9) show the sound pressure to frequency curve of each model. In order to make an comparison, we put SP-00 and 01's sound pressure and power spectrum curve in one diagram, respectively.

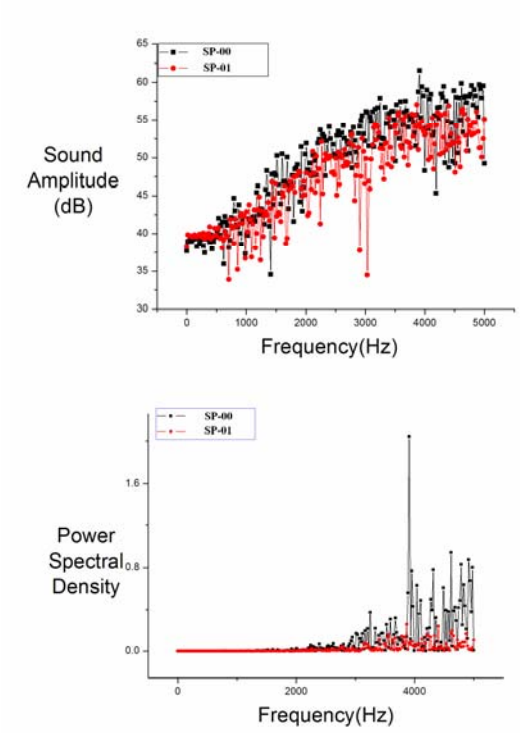

Figure 8 Comparison of power density and sound pressure between SP-00 and 01

Compared with 00 and 01, from Fig. 8 we can see that their power densities have big difference, especially in the high-frequency region, the flat plate's power spectral density can reach nearly 2, but under the same frequency the wavy wall of 01 is only not more than 0.4. This contrast express that the wavy wall has obviously effects of noise reduction than the flat plate. We may also see that all their sound power spectrums are gathered in the range of more than 3000Hz, which indicates that the flow-induced noise performance in our study is mainly manifested as high-frequency. This issue is consistent with that in turbulent flow, the flow-noise are always display as high-frequency.

Fig. 9 shows the variation of other four models' sound pressure in the frequency-field. All of them have the similar growing tendency, and their power density are gathered in the range of 2500Hz to 5000Hz. Combined with Fig. 2, we find that the models who has the effect of drag reduction may not have the same effect in reducing noise, but their variation trends are the same on the whole.

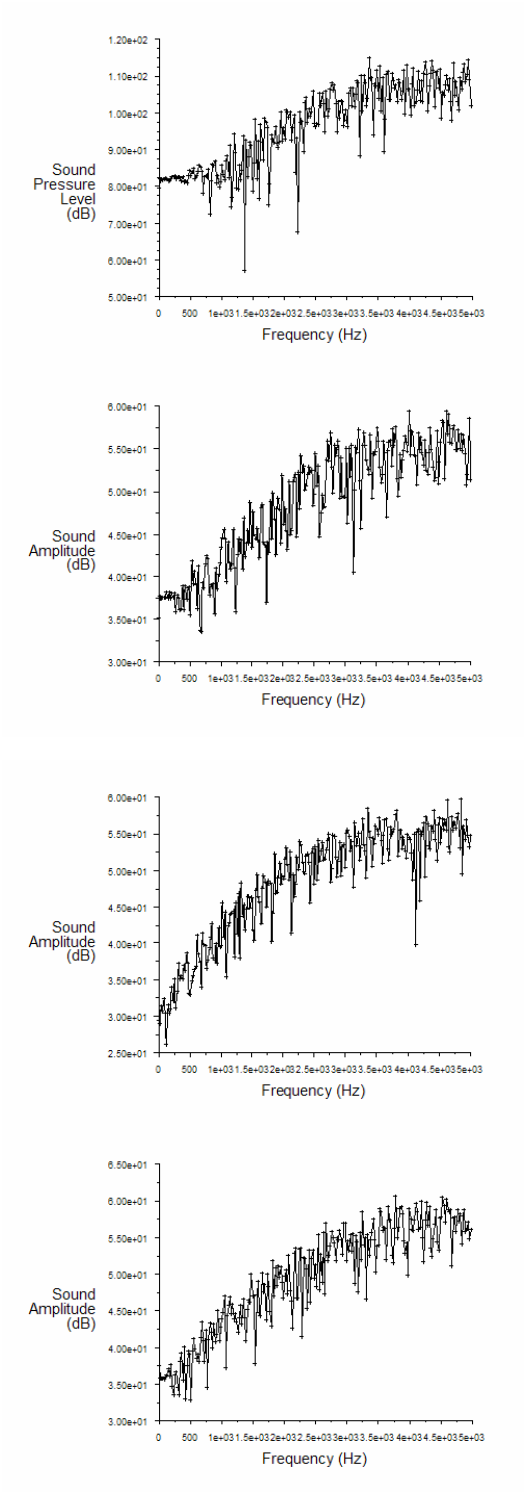

Figure 9 Sound pressure to frequency curves of model SP-02~05

4.2 Case of Streamwise wavy wall

4.2.1 Drag results of streamwise wavy wall

The main dimension of the models in this case is the same as it in the last simulation, but this time the velocity direction of the inflow is changed to be positive $\boldsymbol{x}$. We have simulated many models, because the wave direction is the same as the flow, which makes the flow-field unstable and lead our results of drag seem to be fluctuant. In this case, finally we choose four wavy models which we called ST-001, 002, 003 and 004. The specific characteristics of these models are listed in Tab. 2. And we obtain the drag results of these 5 models as is listed in Tab. 4:

Table 4. Drag results of streamwise wavy wall

ST	a/λ	Pressure drag(N)	frictional drag(N)	Total drag(N)	Total coeffi-cient
000	--	0.000E+00	1.930E-04	1.930E-04	2.311E-03
001	1/200	2.700E-06	2.330E-04	2.360E-04	2.828E-03
002	9/800	1.180E-05	1.890E-04	2.010E-04	2.413E-03
003	1/80	1.460E-05	1.850E-04	2.000E-04	2.398E-03
004	3/200	2.110E-05	1.900E-04	2.110E-04	2.527E-03

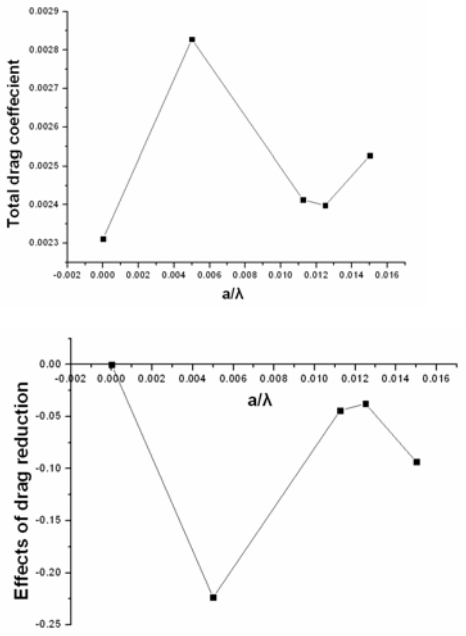

Figure 10 Total drag coefficient and effect of drag reduction results of streamwise wavy wall

What makes us disappointed is that, as is shown in Fig.10, all these models' drag are larger than the flat plate's and they didn't have the effect of drag reduction. Among these wavy walls, model ST-003 has the lowest drag. Either a/λ is larger or lower, they will have a bigger drag. than the flat plate.

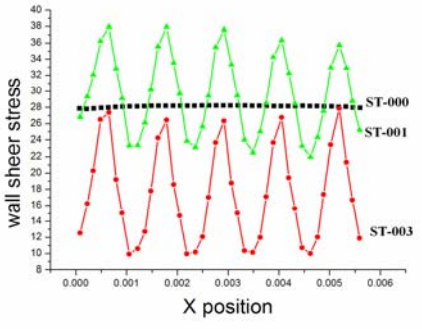

Figure 11 Wall shear stress of 3 models in case of streamwise

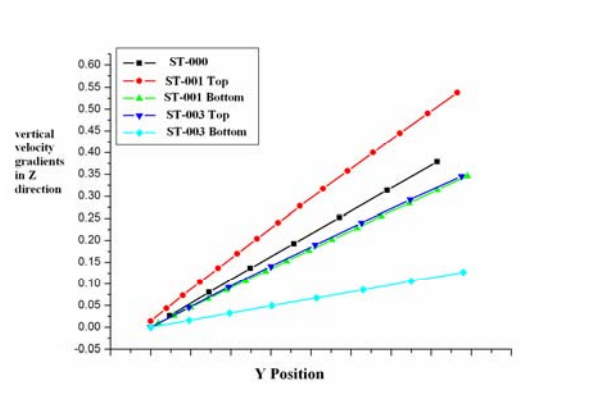

Figure 12 Vertical velocity gradients of 3 models in case of streamwise

Now we should find the reason why these models don't have the effect also from the wall shear stress and the velocity-field. Fig. 11 shows the average, max and min wall shear stress of ST-000, 001 and 003. We found that the shear stress doesn't like it show in the case of spanwise (Fig. 4), where the average value of ST-001 is larger than the flat plate and other models are all lower. The wall shear stress is the reflection of frictional drag, so it can explain the data of frictional drag column in Tab. 4. Fig. 12 shows the vertical velocity gradient distribution of ST-000, 001 and 003. This picture illustrates that why the shear stress are resulted as shown in Fig. 11. The flat plate's velocity is larger than ST-003's, while it is lower than 001's., and this make the shear stress different. From all this analysis we know that both in the case of spanwise and streamwise, the frictional drag could be reduced in some ranges.

Since the shear stress of ST-003 is lower than the flat plate, why its total drag is larger on the other hand? Integrate with Tab. 4, we will find that there isn't a direct relationship between the frictional resistance and the total resistance. But we also know that the total and frictional drag have the same growing trend, and because the pressure drag part in streamwise case is more larger than it is in spanwise, which plays an important role and affects the total drag. This fact gives us a hint that the pressure drag might be the reason why these models do not have drag reduction effect. Further more, for frictional parts of the total drag, either in spanwise or streamwise case, the wavy wall could obtain the drag reducing effect.

4.2.2 Acoustic results of streamwise wavy wall

The following figures (Fig.13~14) show the flow-induced noise results of each model in the case of streamwise wavy wall:

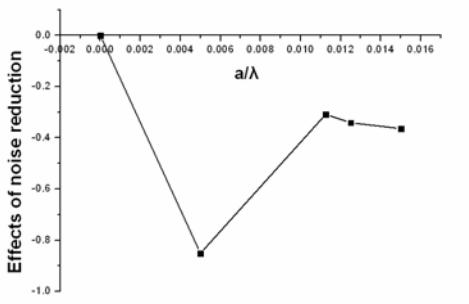

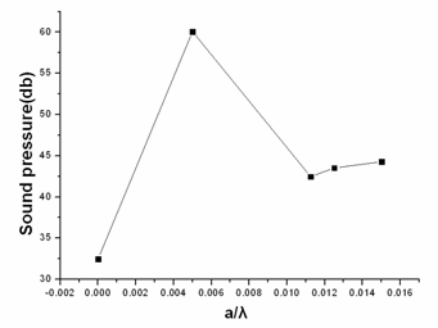

Figure 13 Sound pressure and effect of noise reduction results of streamwise wavy wall

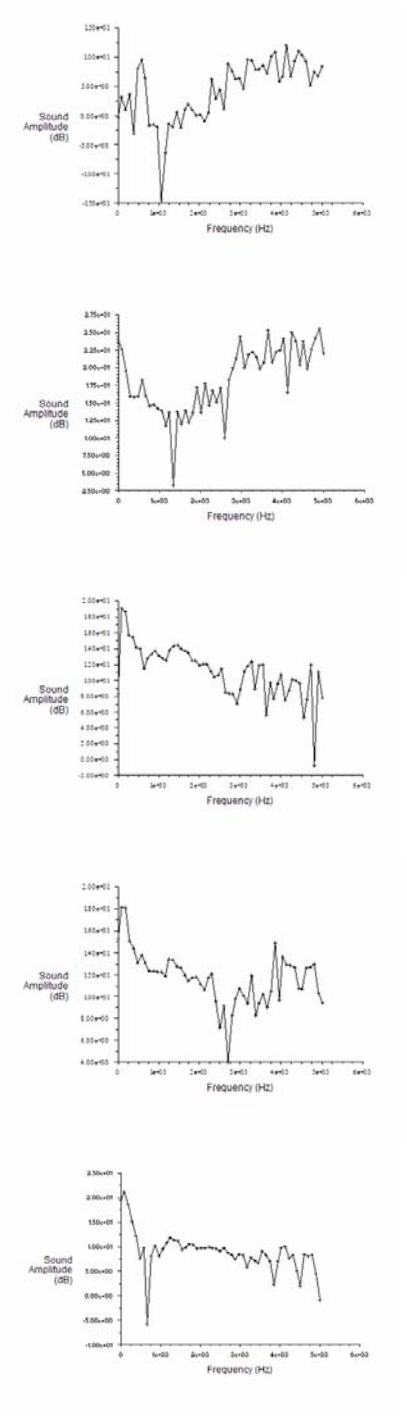

Figure 14 Sound pressure variation by frequency results of models ST 000~004 in case of streamwise

The acoustic results of streamwise, like it is in the drag step, also don't have the effect of noise reduction. Fig. 14 show the flow-induced noise pressure to frequency results of streamwise wavy wall. We can find that each model's growing trend doesn't like it in the case of spanwise (Fig. 8, 9). The power density of the noise in this step usually concentrates in the lower frequency region than it in the spanwise case.

4.3 Summarize

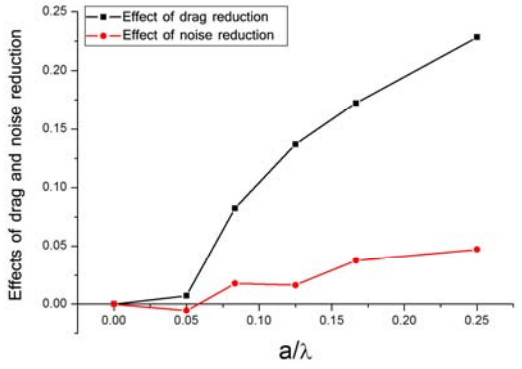

Figure 15 Results of spanwise wavy walls

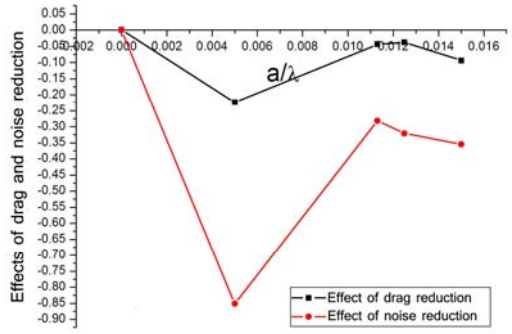

Figure 16 Results of streamwise wavy walls

Fig. 15 shows the result of spanwise wavy walls. In this numerical simulation, It is found that the spanwise wavy walls have both effects of drag and noise reduction, when a/λ= 1/4 the effects are largest. We also find that although the model which has the effect of drag reduction may not have the ability of noise reduction, but their basic variation trends are the same. And if one model has obvious effects on drag reducing, it seems to have the same ability on the soundfield.

Fig. 16 shows that all the streamwise wavy walls have no effects of drag and noise reduction. It is means that the drag and flow noise of the streamwise wavy walls are larger than flat plate. Fig. 16 obviously shows that the relationship between the total drag and noise is very clearly, where their have the same growing trend. These prove that we put the drag and noise together to study the reducing effects with wavy wall is justified.

5. Conclusions

Numerical simulation for drag and noise reduction has been applied to a turbulent flow along wavy wall with various wave amplitude. It is observed that different spanwise wavy wall or streamwise wavy wall caused different skin drag and different flow noise. In some special size of spanwise wavelength, the wavy wall can reduce the skin drag and the flow noise. Different wavelength has different effect of drag and noise reduction.

From the results we may make some conclusions that the spanwise wavy wall surfaces surely have the effect of drag reduction. The main reason is that the existence of the quadratic-vortex can drop the wall shear stress down, which leads to the reducing of frictional drag. When the wave amplitude a and length λ are hold in a suitable range, as their ratio increased, the effect of drag reduction tends to be better. On the other hand, the spanwise wavy wall also can reduce the flow-induced noise. It is a pity that in the streamwise case the drag reduction model didn't appear, but what we find in this case is that the relationship between the total drag and noise is very clearly, where their have the same growing trend.

REFERENCES

1 Walsh, M. J., and Lindemann, A. M., Optimization and Applications of Riblets for Turbulent Drag Reduction. AIAA Paper NO.84-0347,1984.

2 Park, S.-R., and Wallace, J. M., Flow Field Alteration and Viscous Drag Reduction by Riblets in a Turbulent Boundary Layer. In Near-Wall Turbulent Flows, 745-760, Elsevier, 1993.

3 K.-S. Choi, D. M. Orchard, Turbulence management using Riblets for Heat and momentum transfer. Experimental Thermal and Fluid Science, Volume 15, Issue 2, August 1997, Pages 109-124.

4 D.W. Bechert, M. Bruce, W. Hage, J.G.T. Van Der Hoeven, G. Hoppe, Experiments on drag reducing surfaces and their optimization with an adjustable geometry, J. Fluid Mech. 338(1997) 59-87.

5 Lighthill M J., "On sound generated aerodynamically II. Turbulence as a source of sound", Proc Royal Soc London, Ser A, 222, 1-25(1954)

6 Curle N., "The influence of solid boundaries upon aerodynamic sound", Proc Royal Soc London, Ser A, 231, 505-514(1955)

7 Bakewell H P, Carey G F, Libuha J J, et al. Wall pressure correlations in turbulent pipe flow. U.S. Navy Underwater Sound Laboratory Report No.559, 1962

8 Dougls S. Henn and R. Ian Sykes，Large-eddy simulation of flow over wavy surfaces，J. Fluid Mech., 383, 1999, p.75-112

9 Hang Seok Choi , Kenjiro Suzuki，Large eddy simulation of turbulent flow and heat transfer in a channel with one wavy wall, International Journal of Heat and Fluid Flow, 26, 2005, p.681-694

10 Vlachogiannis M., Hanratty T. J.，Influence of wavy structured surfaces and large scale polymerstructures on drag reduction，Experiments in Fluids 36,2004, p.685–700.